

Article

Transient Liquid Phase Bonding of Al-6063 to Steel Alloy UNS S32304 [†]

Mohamed I. Saleh ^{1,*}, Hans J. Roven ², Tahir I. Khan ³ and Terje Iveland ⁴ 

¹ Centre for Advanced Materials, Qatar University, Doha 2713, Qatar

² Department of Materials Science and Engineering, Norwegian University of Science and Technology, 7491 Trondheim, Norway; hans.j.roven@ntnu.no

³ School of Engineering, University of Bradford, Bradford BD7 1DP, UK; T.Khan20@bradford.ac.uk

⁴ Hydro Research and Development Center, P.O. Box 53, 6601 Sunndalsøra, Norway; Terje.Iveland@hydro.com

* Correspondence: misaleh@qu.edu.qa; Tel.: +974-4403-3994; Fax.: +974-4403-3989

[†] This manuscript is extension version of the conference paper: Saleh, M.I.; Khan, T.I.; Roven, H.J. Transient liquid phase bonding of AA-6063 to UNS S32304 using Cu interlayer. In Proceedings of the 5th International Conference on Recent Advances in Materials, Minerals and Environment (RAMM) & 2nd International Postgraduate Conference on Materials, Mineral and Polymer (MAMIP), Penang, Malaysia, 4–6 August 2015.

Received: 5 July 2018; Accepted: 28 August 2018; Published: 1 September 2018



Abstract: Transient liquid phase (TLP) bonding of 6063 aluminum alloy (Al-6063) and duplex alloy 2304 stainless steel (UNS S32304) was performed using copper foil as an interlayer between the base metals. A compression load was applied normal to the specimens. Metallurgical examination of the produced joints showed three distinct regions including a reaction zone, diffusion affected zone, and the base metals. The diffusion of copper into aluminum resulted in an Al–Cu eutectic structure. However, the oxide layer on the aluminum surface controlled the dissolution behavior of copper and the extent of its wettability with the base metals. Although voids and intermetallic compounds were detected at the interfaces of the processed joints, a defect free joint was produced at 570 °C. In addition, the results from corrosion tests showed that the use of copper as an interlayer decreased the corrosion resistance of the joints. However, increase in thickness of the joining reaction zone with increasing bonding temperature was observed to increase corrosion resistance.

Keywords: TLP bonding; eutectic; aluminum alloys; duplex stainless steel

1. Introduction

There is a growing demand for cost-effective materials with enhanced engineered properties. This involves the use of dissimilar metals [1,2]. Although dissimilar metal-couples are being used in the transportation, aerospace, and oil and gas sectors, the bonding of dissimilar metals is still facing numerous challenges and difficulties [1–4]. The difference in thermal expansion coefficients of dissimilar metals can result in residual stresses within the joint region which can eventually cause failure of the joint when conventional fusion welding is used [5]. Furthermore, the large difference in melting point between different metals (e.g., aluminum and steel) makes the use of fusion welding processes difficult to apply to these metals [6,7].

Stub ends, flanges, and pipe fittings are examples of parts and structures, where dissimilar metal joints are used [1,8]. Furthermore, many engineering components where corrosion susceptibility is high, the potential difference between the dissimilar materials is of great concern corrosion [9]. The formation of intermetallic compounds (IMCs) during welding is a challenge for scientists and researchers, such compounds can easily result in brittle fracture of the joints. Therefore, all these factors must be considered in order to produce good dissimilar metal-couples [10–12].

The emerging trend in the automotive industry is to reduce CO₂ emissions by improving the fuel efficiency. Reducing the weight of vehicles is one way of savings in fuel consumption [4,13]. This pressing demand has led to the introduction of lightweight materials such as aluminum alloys into the transportation industry. Aluminum alloys are among the lightest metallic materials promising structures with high specific strength, good corrosion resistance, and excellent recyclability [14,15]. Although the employment of aluminum as the sole material for the manufacturing of vehicles has been successfully achieved, the limited strength of aluminum, as well as the expected cost of production, are among the challenges that resist the commercialization of such a vehicle [16]. On the other hand, steel has been recognized as the most widely used metal in vehicle construction [17]. Thanks to their high elevated-temperature strength, low cost, and good formability [18,19]. Therefore, merging aluminum to steel in a single structure could be a smart approach to combine the beneficial properties of both materials.

Several methods have been applied to bond dissimilar metals in general, and steel and aluminum in particular [1]. Each one has its own advantages and limitations. Selecting the most appropriate method is vital for accomplishing successful joints. Fusion welding processes, solid-state bonding, adhesive bonding, brazing, and soldering are the most well-known methods of bonding dissimilar metals [1,20].

Spot welding has been considered the predominant and the most used welding method in the automotive industry [2]. Qiu et al. (2010) characterized the interface between mild steel and 5052 Al alloy joints made by spot welding. Reaction products of FeAl₃ were detected at the circumferential region of the weld, while FeAl₃ and Fe₂Al₅ were detected beside aluminum and steel respectively at the central region of the weld [21]. Insertion of interlayers between the joining surfaces could suppress the formation of IMCs [1]. Zhang et al. (2014) investigated the effect of interlayer 4047 AlSi12 on the microstructure and mechanical properties of H220YD galvanized high strength steel and 6008-T6 Al alloy joints. It was found that Fe₂(Al,Si)₅ and Fe₄(Al,Si)₁₃ compounds formed at the interface between aluminum and steel. Furthermore, the thickness of IMC formed has an inverse correlation with the interlayer thickness [16].

Joining of Al alloys to steel by laser welding has been investigated and many publications are available in the literature [3,22–25]. Meco et al. (2015) used laser brazing technique to join XF350 steel to AA5083 aluminum alloy. The idea of this process involves applying a laser beam to the steel surface. The heat will be conducted through the steel plate and melt the aluminum to wet the steel and create the joint. It was reported that the welded samples were free from defects although some IMCs such as Fe₂Al₅ and FeAl₃ were detected [22].

Unlike fusion welding, solid-state diffusion brazing does not require melting of base metals. It can also be considered as a versatile process in terms of work piece thickness and geometry [2]. Many researchers have investigated different methods of joining metals and their behaviors [26–28]. Chen and Kovacevic (2004) declared that aluminum 6061 can be joined to mild steel by friction stir welding (FSW) through the combined effect of solid-state and fusion welding. However, several holes were found at the top of the weld and IMCs such as: Al₁₃Fe₄ and Al₅Fe₂, were detected in the nugget zone [29]. Shen et al. (2015) also used FSW technique to join Al5054 plates to DP600 steel plates. Welds with excellent mechanical properties were fabricated. However, intermetallic compound Fe₄Al₁₃ was detected at the fracture zones [30].

In this paper, a feasibility study is undertaken to fabricate joints between Al-6063 and UNS S32304, using a pure Cu foil as an interlayer between the base metals and at a temperature lower than conventional welding processes. The advantage of using Cu between Al and steel is that Cu can make a eutectic reaction with Al, and at the same time one avoids the formation of IMCs with Fe [31].

2. Materials and Methods

UNS S32304 and Al-6063 were supplied by ThyssenKrupp (Nirosta GmbH, Krefeld, Germany) and Qalex (Qatar Aluminium Extrusion Company, Rayyan, Qatar), respectively. Samples were machined

to rectangular dimensions of 30 mm × 15 mm. Aluminum samples were fabricated from an extruded Al-6063 sheet of 2 mm thickness, while duplex stainless steel samples were in the form of coupons with a thickness of 1 mm. A copper foil with 99.9% purity and 10 μm thickness was obtained from Goodfellow, Huntingdon, UK, was used to form an interlayer between the aluminum and stainless steel sheets. The base metal surfaces to be bonded, were ground to 1000 grit surface finish using SiC paper, cleaned with ethanol and dried using hot air. Each joint consisted of two overlapping samples with a piece of copper foil sandwiched in between.

The TLP bonding process was executed using a thermo-mechanical simulator of type Gleeble 3500 (Dynamic Systems Inc., New York, USA), in an inert atmosphere (argon) and a heating rate of 100 °C min⁻¹. A thermocouple wire was welded to the edge of the aluminum sample; approximately in the middle of the overlap region in order to ensure an accurate monitoring of the specimen temperature. A compression load of 0.2 KN was applied to the specimens. The processing temperature to form the joints was varied between 550 °C, 555 °C, 560 °C and 570 °C. Figure 1 shows a sample setup in the Gleeble system.

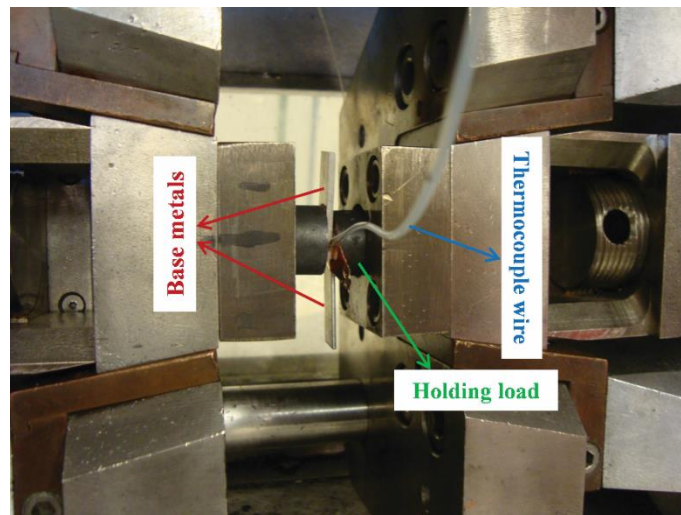


Figure 1. Sample set up for bonding in the Gleeble system [2].

The microstructural development at the joint interface of the copper interlayer was characterized in a scanning electron microscope (SEM, FEI Nova NanoSem 450, Brno, Czech Republic) equipped with energy dispersive X-ray spectroscopy (EDX) and an X-ray diffraction analysis unit (XRD, PANalytical Empyrean, Almelo, The Netherlands). Al-6063 and UNS S32304 were grinded and polished to a 1 μm finish using a diamond suspension. After polishing, Al-6063 was etched with Weck's reagent, while UNS S32304 was etched with Kalling's reagent. An optical microscope (Leica DM IRM, Wetzlar, Germany) equipped with Clemex image analysis software, was used to measure the size of aluminum grains. Micro-hardness measurements across the interface were conducted in accordance to ASTM E384 using a load of 50 g in a Vickers micro-hardness tester (Future-Tech ARS900, Kanagawa, Japan). The hardness profile included 11 points measured from the center of the joint to 500 μm on both sides of the interface. The indentation spacing was 0.1 mm. Further, corrosion rates of the joints were evaluated using potentiodynamic polarization tests in a Gamry 600 potentiostat, and a 3.5% NaCl solution.

3. Results and Discussion

3.1. Microstructural Development in Joints

The resultant area of bonding in various samples can be categorized into three distinct zones (Figure 2), i.e., base metal (Z1), reaction zone (Z2), and diffusion affected zone (Z3); The latter is the area adjacent to Z2 at both sides extending into the Al-6063 and UNS S32304, respectively.

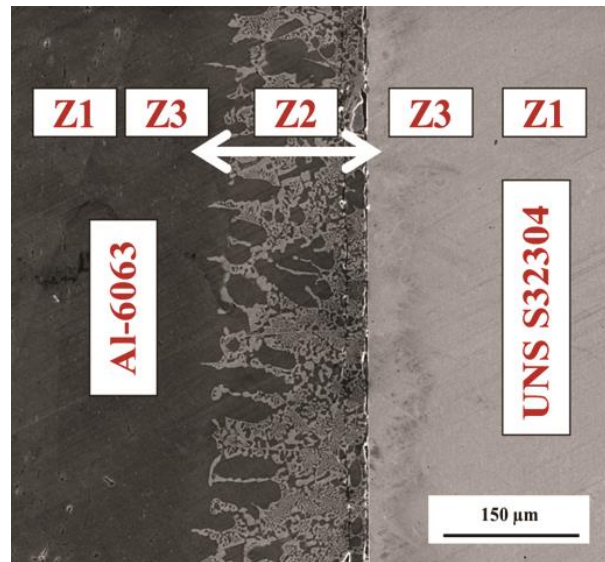


Figure 2. Scanning electron microscope (SEM) micrograph showing resultant reaction zones after the bonding process. (Transient liquid phase (TLP)-560 °C-5 min).

In general, the wettability of liquid Cu on the Al-6063 substrate is relatively high. Hence, liquid copper spread easily along the whole joint interface. On the contrary, the wettability of Cu on UNS S32304 is low and no intermetallic zones formed at the Cu/Fe interface. The formation of Al–Cu eutectic phase occurred at the interface. As soon as the eutectic liquid forms, Cu will tend to diffuse into Al rather than the steel. This occurs as a consequence of the much higher value of the diffusion coefficient of Cu in Al than for Cu in Fe. An undissolved portion of Cu was observed at the joint interface of some samples, while the samples processed at 570 °C showed a defect-free joint with a thick reaction zone having a dense sub-zone closed to the interface (see Figure 3c).

The thickness (Z) of the reaction zone Z2 is a function of temperature (T) and time (t) and can be expressed by the following parabolic equation:

$$Z = (2Kt)^{0.5}$$

and

$$K = K_0 \exp(-Q/RT). \quad (1)$$

Hence, K is the growth velocity (m^2s^{-1}); K_0 a growth constant (m^2s^{-1}); R is the gas constant ($8.314 \text{ KJ mol}^{-1}$); and Q is the activation energy (KJ mol^{-1}) [21,32].

Further, a direct correlation between the bonding temperature and reaction zone thickness could be found, i.e., see Figure 4. The average thickness of Z2 increased from 96 μm at 550 °C to 217 μm at 570 °C.

Figure 5 shows the location of the EDX analysis and the corresponding, chemical compositions, across the interface, respectively. The diffusion coefficients of Cu in Al ($D_{\text{Cu} \rightarrow \text{Al}}$) and Cu in Fe ($D_{\text{Cu} \rightarrow \text{Fe}}$), at same temperature, are about six order of magnitude different. Therefore one observed that Cu diffused more easily into the Al-alloy than the steel [31,33]. In comparison, insignificant amounts of

Cu (≈ 0.8 at.%) were detected in points D and E, e.g., along the joint interface at the UNS S32304 side. The stainless steel bonded at 570 °C, absorbed Cu to a content close to 0.8% (see Figure 5). In fact, in the literature it was reported that the solubility of Cu in Fe can be enhanced by raising the bonding temperature [31].

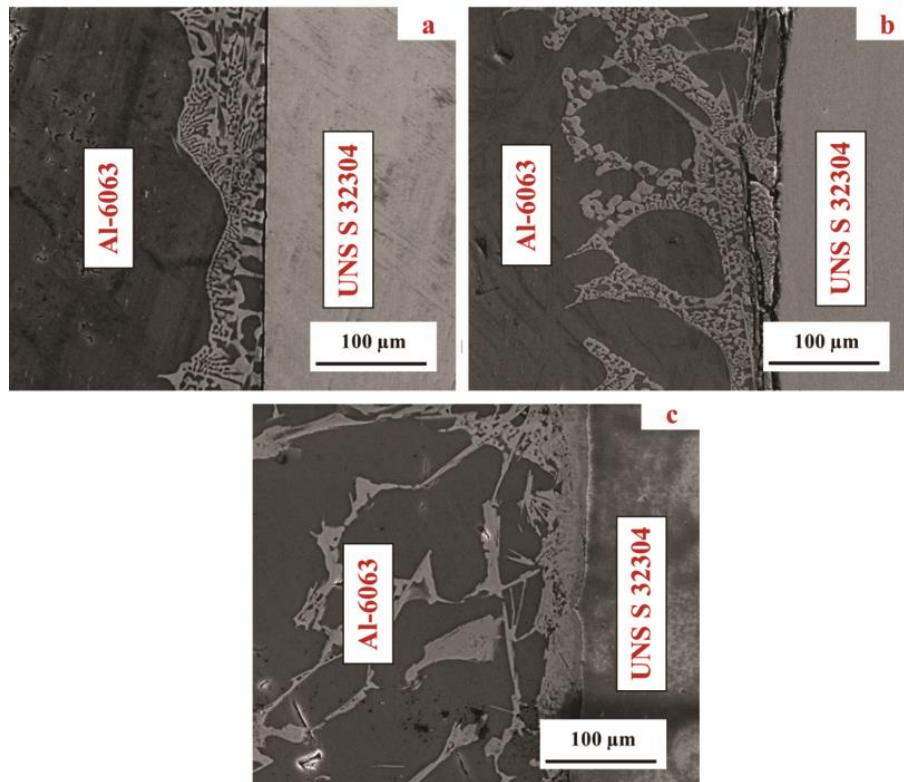


Figure 3. SEM micrographs of Al-6063-UNS S32304 joint interface produced by TLP bonding at (a) 550 °C; (b) 555 °C; (c) 570 °C.

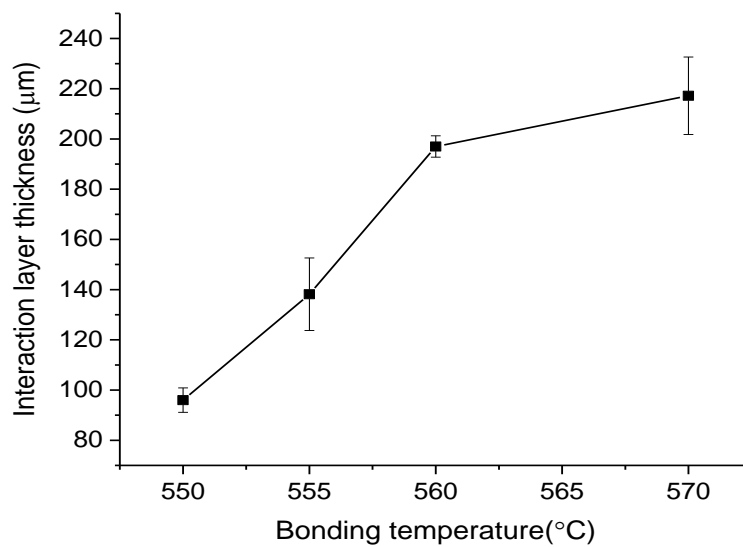


Figure 4. The relationship between bonding temperature and thickness of the reaction zone.

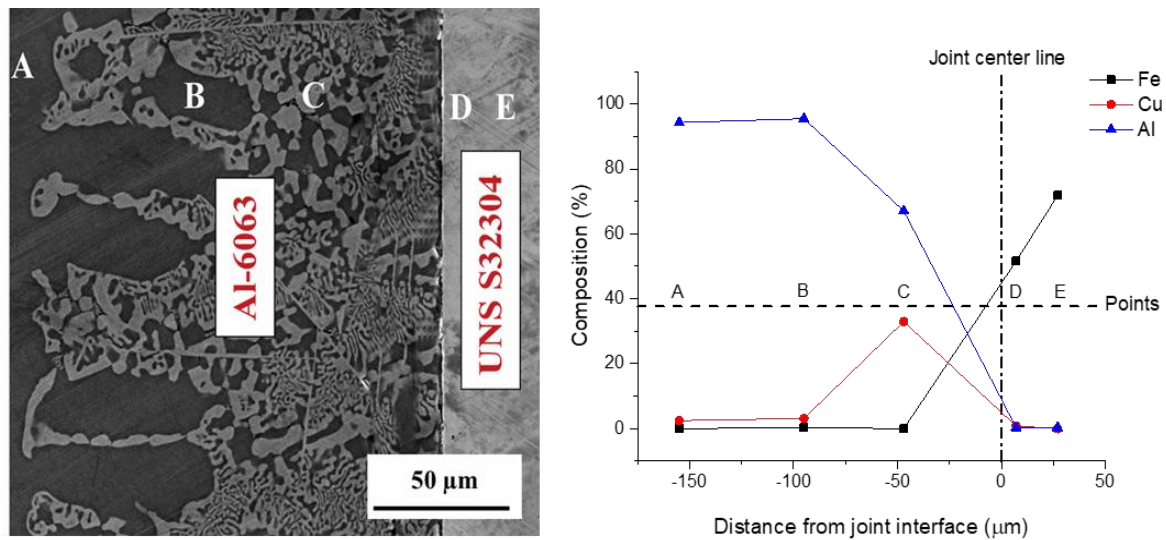


Figure 5. SEM micrograph and energy dispersive X-ray spectroscopy (EDX) analysis of five selected points (A to E) (TLP-560 °C-5 min).

The highest Cu concentration between 28–33 at.% was observed at Point C, located in the Al-alloy. Furthermore, diffusion of Cu extended into the Al-alloy away from the joint. The decrease in Cu content at the joint interface resulted in isothermal solidification at the eutectic temperature [34].

Moreover, diffusion of Fe into Al was also observed. An approximate amount of 0.3 at.% of Fe was detected at point B. The lowest percentage of Al detected at points D and E were 0.32 and 0.31 at.%, respectively, which is due to the large difference in the diffusion coefficients between Fe in Al ($D_{\text{Fe} \rightarrow \text{Al}} = 1.00 \times 10^{-13} \text{ m}^2 \text{ s}^{-1}$) and Al in Fe ($D_{\text{Al} \rightarrow \text{Fe}} = 9.94 \times 10^{-19} \text{ m}^2 \text{ s}^{-1}$) [13].

The shown XRD pattern revealed the existence of Al_2Cu at the interface near the Al-6063 side (see Figure 6). This is in good agreement with the EDX data (Figure 5). The presence of FeAl_3 as indicated by Sun et al. (2015) has not been observed in the present case, which is presumably because Cu acted as a transition material between Al and Fe, preventing direct contact and hence suppressing the formation of Fe–Al intermetallic compounds [24].

The highest magnification view of the microstructure shown in Figure 7 indicates that Cu diffused from the joint interface into the Al-alloy along grain boundaries. Therefore, one can claim that grain boundary diffusion is dominant over lattice diffusion during the present bonding process.

The diffusion path depends on several factors such as microstructure, temperature and the interface quality between the metal and adjacent layers [35]. The Arrhenius' law describes the effect of activation energy (E_a) on the diffusion coefficient (D):

$$D = D_0 e^{-E_a/RT}. \quad (2)$$

Grain boundary diffusion has a fast diffusion path due to the open structures of the boundaries. The latter formed a network along the whole area of the specimen. Also, voids and imperfections along Al grain boundaries render the diffusion of Cu easier than diffusion through the lattice [35–37].

Figure 8 shows the microstructure of UNS S32304 steel before and after the bonding process. Unlike Al, because of the presence of Cu, the etching process was more aggressive on the post-welded samples than the as-received ones. It was also noticed that ferrite grains ($\alpha\text{-Fe}$) were significantly more etched than the austenite grains ($\gamma\text{-Fe}$). This could be attributed to the significant difference between Cu diffusivities in $\alpha\text{-Fe}$ and $\gamma\text{-Fe}$ (4.4×10^{-9} and $9.4 \times 10^{-12} \text{ cm}^2 \text{ s}^{-1}$, respectively). In addition, $\alpha\text{-Fe}$ (BCC) has a more open atomic structure than $\gamma\text{-Fe}$ (FCC) [37,38].

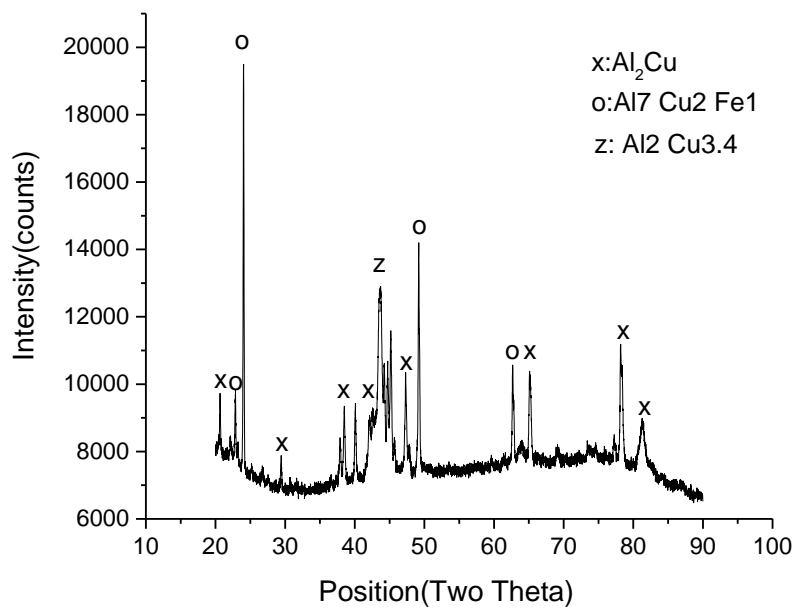


Figure 6. X-ray diffraction analysis unit (XRD) spectrum of the eutectic region of a TLP joint.

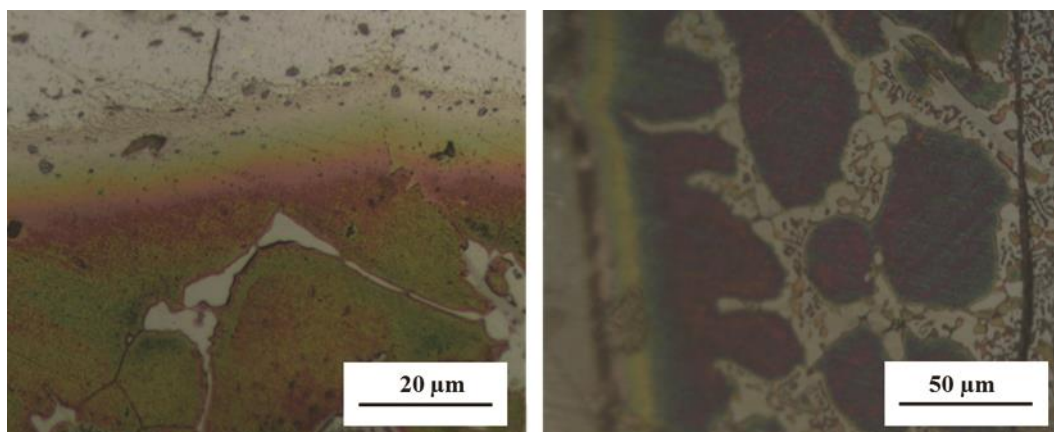


Figure 7. Close-up of microstructure of Al-6063 in zone Z2 after the bonding process [2].

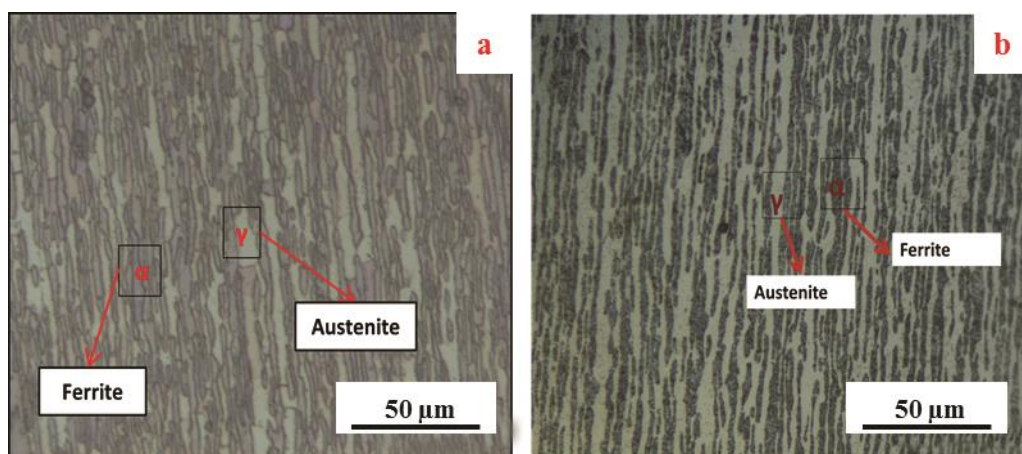


Figure 8. Austenite and ferrite grains of UNS S32304 (a) before the bonding process; (b) after the bonding process at (550–570 °C) [2].

3.2. Micro-Hardness Evaluation

Figure 9 shows the micro-hardness profile for samples made by TLP bonding at 550 °C, 555 °C, 560 °C, and 570 °C. The average micro-hardness values at the joint interface were in the range of 125–175 HRB. A gradual decrease in the hardness occurred away from the interface, towards the Al-6063 side. The micro-hardness of Al-6063 decreased after a distance of 200 μm from the joint interface by 44–50% (from an average of 132 HRB to 58–67 HRB). The higher hardness of the post-welded Al-6063 was due to diffusion of Cu [39]. Furthermore, the joint formed at 570 °C exhibited a significant increase in hardness within the Al-6063 alloy compared to the other joints made at lower temperatures. This is due to the maximum spread of the eutectic phase for the joint produced at 570 °C. On the UNS S32304 side, the micro-hardness profile gave an average value of 266 HRB in a position 200 μm from the joint interface.

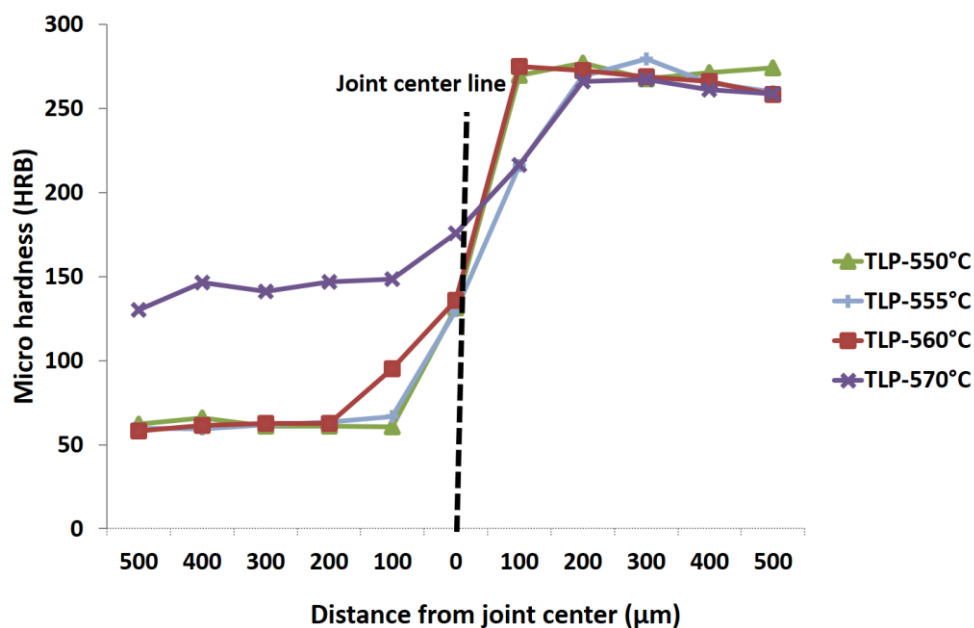


Figure 9. Micro-hardness profile of joints made by TLP bonding at various temperatures. The Al-alloy and steel alloy to the left and right, respectively.

3.3. Corrosion Resistance

The potentiodynamic polarization curves for TLP bonding joints as a function of bonding temperature are shown in Figure 10. I_{corr} and E_{corr} were calculated by extrapolating the tafel plots of each test to the zero potential. Each test was repeated twice and found to be reproducible. As shown in Figure 10, all the joints exposed to the same experimental condition, showed similar behavior in the polarization test. However, I_{corr} decreased at higher bonding temperature with the lowest I_{corr} value obtained for the joint produced at 570 °C. It was found that the thickness of the reaction zone had a direct relation with the bonding temperature (see Figure 4). Therefore, the joint produced at 570 °C formed the thickest reaction zone compared to other joints formed at lower temperatures. According to the findings in [40], the denser the reaction zone, the higher the corrosion resistance of the joint. The present polarization curves in Figure 10 clearly confirmed these observations. The shift in curves to a more positive potential with increasing bonding temperature from 550 °C to 570 °C indicated a better corrosion resistance of the joint.

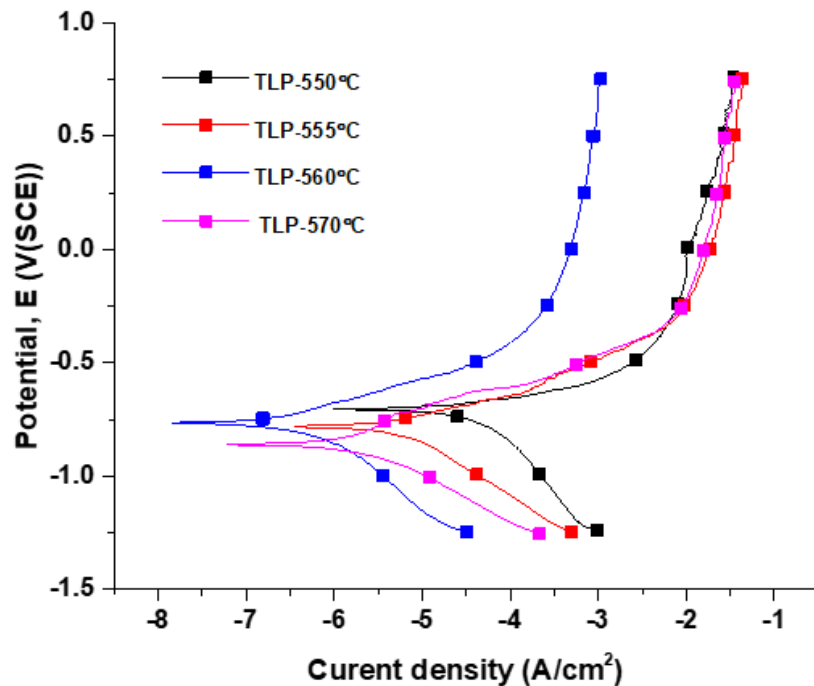


Figure 10. Comparison of polarization curves for TLP bonding joints produced at various temperatures.

4. Conclusions

Transient liquid phase bonding of Al-6063 to UNS S32304 was studied using a thin Cu interlayer. The effects of the Cu interlayer and bonding temperature (550 °C, 555 °C, 560 °C, and 570 °C) on the microstructure, corrosion resistance and micro-hardness of the resulting joints were investigated.

- The resultant area of TLP bonding consisted of three distinct zones including base metal, reaction zone and diffusion affected zone. Cu diffused into the Al alloy and formed an eutectic phase. However, no reaction was observed on the UNS S32304 side.
- As the bonding temperature increased from 550 °C to 570 °C, the thickness of the reaction zone increased by over 100%.
- Although voids and intermetallic compounds (Al_2Cu) were found at the interface, a TLP joint was produced successfully at 570 °C.
- Employing Cu foil as an interlayer suppressed the formation of Fe–Al intermetallics.
- Hardness was increased on the Al-6063 side as a result of Cu diffusion. However, changes in hardness for the UNS S32304 steel was negligible.

Supplementary Materials: The Estimation of the dissolution time and rate of the Cu interlayer is available online at <http://www.mdpi.com/2504-4494/2/3/58/s1>.

Author Contributions: Conceptualization, T.K., M.S. and H.R.; Methodology, M.S and T.I; Writing-Original Draft Preparation, M.S; Writing-Review & Editing, T.K and H.R.; Supervision, T.K and H.R.; Funding Acquisition, H.R. and M.S.

Funding: This research was funded by Qatar Aluminum Limited (Qatalum) grant number [M-034].

Acknowledgments: The authors would like to acknowledge Qatalum for funding this work. The authors are also thankful to the technical staff at Hydro Research and Technology Development Center in Norway for their support.

Conflicts of Interest: The authors declare no conflict of interest.

References

1. Martinsen, K.; Hu, S.J.; Carlson, B.E. Joining of dissimilar materials. *CIRP Ann.* **2015**, *64*, 679–699. [CrossRef]
2. Saleh, M.I.; Khan, T.I.; Roven, H.J. Transient liquid phase bonding of AA-6063 to UNS S32304 using Cu interlayer. *Procedia Chem.* **2016**, *19*, 517–524. [CrossRef]
3. Chen, H.-C.; Pinkerton, A.J.; Li, L.; Liu, Z.; Mistry, A.T. Gap-free fibre laser welding of Zn-coated steel on Al alloy for light-weight automotive applications. *Mater. Des.* **2011**, *32*, 495–504. [CrossRef]
4. Sakiyama, T.; Naito, Y.; Miyazaki, Y.; Nose, T.; Murayama, G.; Saita, K.; Oikawa, H. Dissimilar metal joining technologies for steel sheet and aluminum alloy sheet in auto body. *Nippon Steel Tech. Rep.* **2013**, *103*, 91–98.
5. Paul, K.; Shrestha, M.; Martikainen, J. Trends in Joining Dissimilar Metals by Welding. *Appl. Mech. Mater.* **2013**, *440*, 269–276. [CrossRef]
6. Sierra, G.; Peyre, P.; Deschaux Beaume, F.; Stuart, D.; Fras, G. Galvanised steel to aluminium joining by laser and GTAW processes. *Mater. Charact.* **2008**, *59*, 1705–1715. [CrossRef]
7. Mei, S.W.; Gao, M.; Yan, J.; Zhang, C.; Li, G.; Zeng, X.Y. Interface properties and thermodynamic analysis of laser–arc hybrid welded Al/steel joint. *Sci. Technol. Weld. Join.* **2013**, *18*, 293–300. [CrossRef]
8. Findik, F. Recent developments in explosive welding. *Mater. Des.* **2011**, *32*, 1081–1093. [CrossRef]
9. Prawoto, Y. Synergy of erosion and galvanic effects of dissimilar steel welding: Field failure analysis case study and laboratory test results. *J. King Saud Univ. Eng. Sci.* **2013**, *25*, 59–64. [CrossRef]
10. Muralimohan, C.H.; Haribabu, S.; Reddy, Y.H.; Muthupandi, V.; Sivaprasad, K. Evaluation of Microstructures and Mechanical Properties of Dissimilar Materials by Friction Welding. *Procedia Mater. Sci.* **2014**, *5*, 1107–1113. [CrossRef]
11. Dissimilar Materials Joining. Available online: <https://ewi.org/dissimilar-materials-joining/> (accessed on 6 May 2018).
12. Torbati, A.M.; Miranda, R.M.; Quintino, L.; Williams, S.; Yapp, D. Optimization procedures for GMAW of bimetal pipes. *J. Mater. Process. Technol.* **2011**, *211*, 1112–1116. [CrossRef]
13. Watanabe, T.; Doi, Y.; Yanagisawa, A.; Konuma, S. Resistance Spot Welding of Mild Steel to Al-Mg Alloy. *Q. J. Jpn. Weld. Soc.* **2005**, *23*, 491–495. [CrossRef]
14. Hirsch, J. Recent development in aluminium for automotive applications. *Trans. Nonferrous Met. Soc. China* **2014**, *24*, 1995–2002. [CrossRef]
15. Hirsch, J.; Al-Samman, T. Superior light metals by texture engineering: Optimized aluminum and magnesium alloys for automotive applications. *Acta Mater.* **2013**, *61*, 818–843. [CrossRef]
16. Zhang, W.; Sun, D.; Han, L.; Liu, D. Interfacial microstructure and mechanical property of resistance spot welded joint of high strength steel and aluminium alloy with 4047 AlSi12 interlayer. *Mater. Des.* **2014**, *57*, 186–194. [CrossRef]
17. Yuan, X.; Sheng, G.; Luo, J.; Li, J. Microstructural characteristics of joint region during diffusion-brazing of magnesium alloy and stainless steel using pure copper interlayer. *Trans. Nonferrous Met. Soc. China* **2013**, *23*, 599–604. [CrossRef]
18. Elthalabawy, W.M.; Khan, T.I. Microstructural development of diffusion-brazed austenitic stainless steel to magnesium alloy using a nickel interlayer. *Mater. Charact.* **2010**, *61*, 703–712. [CrossRef]
19. Araki, T.; Koba, M.; Nambu, S.; Inoue, J.; Koseki, T. Reactive Transient Liquid Phase Bonding between AZ31 Magnesium Alloy and Low Carbon Steel. *Mater. Trans.* **2011**, *52*, 568–571. [CrossRef]
20. Shah, L.H.; Ishak, M. Review of Research Progress on Aluminum–Steel Dissimilar Welding. *Mater. Manuf. Processes* **2014**, *29*, 928–933. [CrossRef]
21. Qiu, R.; Shi, H.; Zhang, K.; Tu, Y.; Iwamoto, C.; Satonaka, S. Interfacial characterization of joint between mild steel and aluminum alloy welded by resistance spot welding. *Mater. Charact.* **2010**, *61*, 684–688. [CrossRef]
22. Meco, S.; Pardal, G.; Ganguly, S.; Williams, S.; McPherson, N. Application of laser in seam welding of dissimilar steel to aluminium joints for thick structural components. *Opt. Lasers Eng.* **2015**, *67*, 22–30. [CrossRef]
23. Mathieu, A.; Shabadi, R.; Deschamps, A.; Surey, M.; Mattei, S.; Grevey, D.; Cicala, E. Dissimilar material joining using laser (aluminum to steel using zinc-based filler wire). *Opt. Lasers Eng.* **2007**, *39*, 652–661. [CrossRef]
24. Sun, J.; Yan, Q.; Gao, W.; Huang, J. Investigation of laser welding on butt joints of Al/steel dissimilar materials. *Mater. Des.* **2015**, *83*, 120–128. [CrossRef]

25. Kouadri-David, A. Study of metallurgic and mechanical properties of laser welded heterogeneous joints between DP600 galvanised steel and aluminium 6082. *Mater. Des.* **2014**, *54*, 184–195. [[CrossRef](#)]
26. Ren, J.; Li, Y.; Feng, T. Microstructure characteristics in the interface zone of Ti/Al diffusion bonding. *Mater. Lett.* **2002**, *56*, 647–652. [[CrossRef](#)]
27. Sammaiah, P.; Suresh, A.; Tagore, G.R.N. Mechanical properties of friction welded 6063 aluminum alloy and austenitic stainless steel. *J. Mater. Sci.* **2010**, *45*, 5512–5521. [[CrossRef](#)]
28. Jafarian, M.; Khodabandeh, A.; Manafi, S. Evaluation of diffusion welding of 6061 aluminum and AZ31 magnesium alloys without using an interlayer. *Mater. Des.* **2015**, *65*, 160–164. [[CrossRef](#)]
29. Chen, C.M.; Kovacevic, R. Joining of Al 6061 alloy to AISI 1018 steel by combined effects of fusion and solid state welding. *Int. J. Mach. Tools Manuf.* **2004**, *44*, 1205–1214. [[CrossRef](#)]
30. Shen, Z.; Chen, Y.; Haghshenas, M.; Gerlich, A.P. Role of welding parameters on interfacial bonding in dissimilar steel/aluminum friction stir welds. *Eng. Sci. Technol.* **2015**, *18*, 270–277. [[CrossRef](#)]
31. Atabaki, M.M.; Wati, J.N.; Idris, J. Transient liquid phase diffusion brazing of stainless steel 304. *Weld. J.* **2013**, *92*, 57–63.
32. Guo, W.; Zhao, X.; Song, M.; Fing, J.; Yang, B. Diffusion bonding of Ti-6 Al-4 V to QAl 10-3-1.5 with Ni/Cu interlayers. *J. Mater. Sci. Technol.* **2006**, *22*, 817–820.
33. Na, H.; Kim, J.; Jeong, B.; Kang, C. Effect of brazing conditions on the microstructure and mechanical properties of duplex stainless steels to Cr–Cu alloy with Cu– base insert metal. *Met. Mater. Int.* **2007**, *13*, 511–515. [[CrossRef](#)]
34. Wu, M.-F.; Si, N.-C.; Chen, J. Contact reactive brazing of Al alloy/Cu/stainless steel joints and dissolution behaviors of interlayer. *Trans. Nonferrous Met. Soc. China* **2011**, *21*, 1035–1039. [[CrossRef](#)]
35. Orto, R.L.D. *Electromigration Modeling and Simulation*; Technical University of Vienna: Vienna, Austria, 2010.
36. Suzuki, A.; Mishin, Y. Atomic mechanisms of grain boundary diffusion: Low versus high temperatures. *J. Mater. Sci.* **2005**, *40*, 3155–3161. [[CrossRef](#)]
37. Padron, T.; Khan, T.I.; Kabir, M.J. Modelling the transient liquid phase bonding behaviour of a duplex stainless steel using copper interlayers. *Mater. Sci. Eng. A* **2004**, *385*, 220–228. [[CrossRef](#)]
38. Roberts, G.A.; Krauss, G.; Kennedy, R.L. *Tool Steels*, 5th ed.; ASM International: Geauga, OH, USA, 1998.
39. Porter, D.L.; Totemeier, T.C. 22-Mechanical properties of metals and alloys. In *Smithells Metals Reference Book*, 2nd ed.; Gale, W.F., Totemeier, T.C., Eds.; Butterworth-Heinemann: Oxford, UK, 2004.
40. Khan, T.I.; Kabir, M.J.; Bulpett, R. Effect of transient liquid-phase bonding variables on the properties of a micro-duplex stainless steel. *Mater. Sci. Eng. A* **2004**, *372*, 290–295. [[CrossRef](#)]



© 2018 by the authors. Licensee MDPI, Basel, Switzerland. This article is an open access article distributed under the terms and conditions of the Creative Commons Attribution (CC BY) license (<http://creativecommons.org/licenses/by/4.0/>).